

## Optical hole burning in ruby

P. E. Jessop, T. Muramoto,\* and A. Szabo

*Division of Electrical Engineering, National Research Council of Canada, Ottawa, Canada K1A 0R8*

(Received 23 July 1979)

We report experimental and theoretical studies of optical hole burning in the inhomogeneous  $R_1$  line of ruby at low temperatures. Both Stark-shifting and pump-probe techniques using narrow-band single-frequency lasers were employed. In addition to the observation of narrow holes, we have found that a large (up to 70%) decrease in absorption occurs outside the hole and that the relative size of this decrease is constant over the entire inhomogeneous line. This effect is ascribed to fast resonant cross-spin relaxation in the ground-state levels which drives all spins within the optically pumped volume to a common spin temperature. A theoretical model is formulated which describes the power-broadened hole shapes as well as the off-resonance decrease in the absorption coefficient. Fair agreement with experiment is obtained for the case of a magnetic field applied along the  $c$  axis; however, sizable deviations from the theory are seen for zero field. We conclude that further studies are needed to elucidate the nature of the Al superhyperfine-broadening mechanism. An upper limit of 1200 nm is deduced for the size of macroscopically broadened regions in ruby.

### I. INTRODUCTION

There has been increasing interest recently in optical-hole-burning and fluorescence-line-narrowing (FLN) studies of inhomogeneously broadened lines in solids. The resolution of these laser techniques is limited ultimately by the homogeneous rather than the inhomogeneous widths. Therefore, high-resolution Zeeman,<sup>1</sup> Stark,<sup>2-4</sup> and strain-broadening spectroscopy become possible. Such studies have recently allowed measurements of small hyperfine splittings of optical transitions of ions in crystals<sup>5</sup> and have given information on line-broadening mechanisms.<sup>1,5</sup> These experiments compliment similar studies using coherence techniques.<sup>6,7</sup> Also of interest are various phenomena in the area of hole burning. These include short-time phenomena, such as the cross-relaxation effects described in this and earlier work,<sup>8</sup> as well as long-lived effects, for example photochemical hole burning in organic solids<sup>9,10</sup> and color centers.<sup>11</sup> Higher-resolution spectroscopy is possible with hole burning than with FLN because in the latter technique resolution is limited by the interferometer. With hole burning, resolution is limited only by the laser stability. Finally, there is increasing interest in the possibility of using hole burning for a high capacity, frequency-selective optical memory.<sup>12</sup>

In this paper we extend earlier studies<sup>8</sup> of ground-state cross-relaxation effects on optical hole burning of the  $R_1$  line in ruby. Previously a sideband-spectroscopy technique was used. The frequency coverage of the optical probe used to study the hole was limited to  $\pm 30$  MHz about the hole. Here we describe two additional techniques, one of which has

allowed us to make probe observations over the entire inhomogeneous [ $\sim 2$  GHz FWHM (full width at half maximum)]  $R_1$  line at 693.4 nm when a hole is burnt into it by a narrow-band ( $< 2$  MHz jitter peak to peak) single-mode, cw ruby laser. In addition to the hole, a large (up to 70%) decrease of absorption coefficient is seen over the *entire* inhomogeneous line, unequivocally indicating the presence of spatial transport processes. In this paper we present a detailed theoretical and experimental study of this surprising effect.

In Sec. II we describe experiments using a Stark-switching technique to measure the hole shape. Additional hole-burning studies are reported in Sec. III in which two separate lasers were used, one to saturate and one to probe the hole. In Sec. V, a physical model and theoretical description of hole burning is presented. In Secs. VI and VII, a detailed comparison between theory and experiment is presented along with a discussion of implications for macroscopic versus microscopic inhomogeneous broadening in ruby.

### II. STARK STUDIES

#### A. Introduction

When an electric field is applied along the  $c$  axis of ruby, a linear "pseudo"-Stark splitting<sup>13</sup> is observed for the  $\text{Cr}^{3+}R_1$  and other lines. There are two kinds of sites occupied by the  $\text{Cr}^{3+}$  ions in  $\text{Al}_2\text{O}_3$  which are related to each other by inversion symmetry. The  $R_1$  line associated with each site shifts linearly with field, in opposite directions, to produce the pseudo-Stark-splitting. In this section we describe experiments

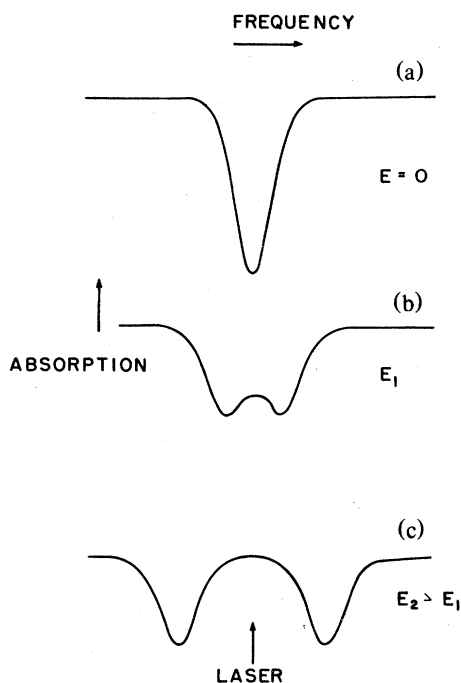


FIG. 1. Stark-shifting technique for measuring hole shape. (a) (top) shows the hole in zero field. In (b) and (c) successively larger electric field pulses shift the hole increasingly above and below the laser frequency.

which use the Stark effect to measure optical hole shapes in the  $R_1$  line of ruby.

The basic idea of the method<sup>2</sup> is shown in Fig. 1. In Fig. 1(a) we show a hole burnt into an inhomogeneous line for zero electric field. If now a step-function electric field is pulsed on, in Figs. 1(b) and 1(c), the hole splits and shifts to higher and lower frequencies. Thus the hole can be scanned through the laser frequency either point by point as in this paper and earlier<sup>2</sup> work or by the continuous tuning.<sup>3</sup> In the present experiments, the hole was measured by monitoring the change in transmitted light when the field was pulsed on.

#### B. Stark switching—experimental

The experimental setup is shown in Fig. 2. A single-frequency laser beam produced by a cw ruby laser is focused into the ruby sample along the  $c$  axis. The electric and magnetic fields are applied along the  $c$  axis. In all the experiments reported in this paper, a Czochralski-grown ruby sample, 1.5 mm thick containing 0.03 wt. %  $\text{Cr}_2\text{O}_3$  (as specified by the manufacturer, Union Carbide) was used. The sample temperature was measured by a Lakeshore silicon diode thermometer attached to the copper structure holding

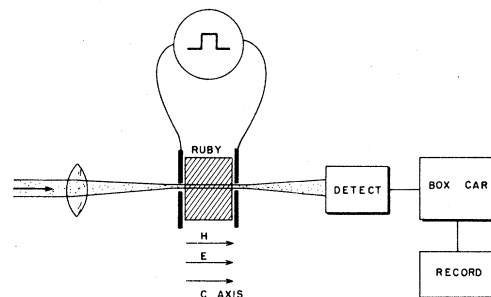


FIG. 2. Schematic of apparatus setup for Stark-shifting experiments.

the crystal. Most experiments were done at a temperature of  $\sim 5$  K. A transparent conducting coating, antireflection coated to give a transmission of 86% at 6900 Å, was applied to two surfaces of the ruby sample to provide the electrodes. The electric field signal was applied through a pair of coaxial transmission lines with the output line being terminated in 50 ohms.

Tuning of the laser in the vicinity of the  ${}^4A_2(\pm \frac{1}{2}) \rightarrow \bar{E}(\pm \frac{1}{2})$  transitions was achieved by temperature control of the laser ruby. The laser beam was circularly polarized and only the  ${}^4A_2(-\frac{1}{2}) \rightarrow \bar{E}(-\frac{1}{2})$  transition was studied. Usually the laser frequency was fixed within  $\sim 100$  MHz of the peak of this line.

A measurement of the Stark splitting using FLN is shown in Fig. 3. Since only a pseudo splitting<sup>13</sup> occurs, the electric field must be pulsed in order to observe the Stark-shifted FLN. We used square-wave modulation at 10 kHz, a rate sufficiently high to minimize  $\bar{E}$  relaxation effects. As expected, each of

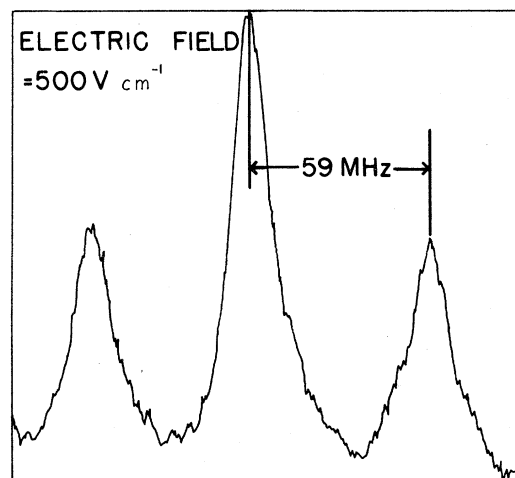


FIG. 3. Measurement of Stark splitting in ruby at 5 K using fluorescence line narrowing. The Stark lines appear symmetrically displaced about the center unshifted line.

the two Stark lines has half the intensity of the unshifted line. The observed<sup>2</sup> shift of the lines is  $0.110 \pm 0.008 \text{ MHz/V cm}^{-1}$ . The slight asymmetry of the Stark-line positions in Fig. 3 about the unshifted line arises from drift of the laser frequency and Fabry-Perot interferometer spacing during the scan. Several scans were averaged to give the quoted Stark coefficient. Our value is consistent with an earlier result,<sup>13</sup>  $0.114 \text{ MHz/V cm}^{-1}$  obtained by a nonlaser technique.

The beam-collection geometry is shown in Fig. 4. This geometry was devised to allow an accurate measurement of the beam intensity and to restrict observations to the central 10% of the beam to avoid edge effects. The intensity in the center of the beam in the sample is

$$I_c = \left( \frac{d}{\lambda L} \right)^2 \frac{\pi P_0}{F_d}, \quad (1)$$

where  $P_0$  is the total beam power,  $F_d$  is the fraction of power transmitted through the aperture diameter  $d$ , and  $L$  is the distance between the aperture and focal plane. We chose  $d$  sufficiently small that the intensity was approximately constant in the aperture.

A reed-switched transmission-line pulser supplied a rectangular voltage pulse, 400 nsec in width and with a height which was variable up to 100 volts. A PAR 162 boxcar with a 10-nsec gate averaged the signal at a 80-Hz repetition rate. This gave a duty factor of  $3 \times 10^{-5}$  during the pulse for an average probe power far below the value of  $0.1 \text{ W/cm}^2$  for which saturation effects begin to appear.<sup>8</sup> The signal level corresponding to a transparent sample was measured by heating the sample to 120 K which moves the  $R_1$  line 43 GHz out of resonance with the laser. The unsaturated absorption coefficient  $\alpha_\mu$  was measured by recording the decrease in the transmission of a low-power laser beam as the sample was cooled from 120 K back to 5 K. A value of  $\alpha_\mu = 11.0 \pm 0.4 \text{ cm}^{-1}$  was determined from the observed attenuation of 5.2 in our 1.5-mm-thick sample. Data showing the frequency dependence of the hole shapes, obtained by scanning the electric field pulse amplitude, are shown in Fig. 5 for various laser intensities in the sample.

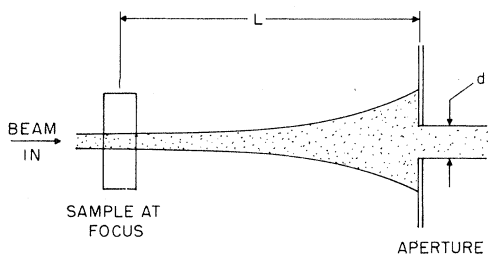


FIG. 4. Laser-beam collection geometry used to observe only the central part of the beam in Stark experiments.

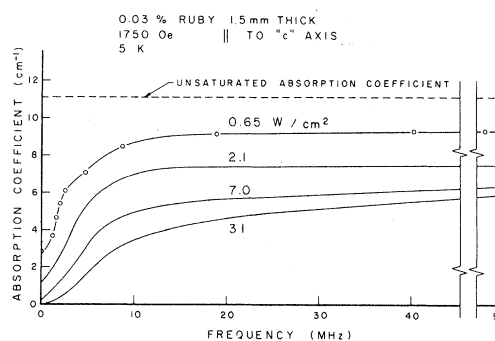


FIG. 5. Experimental hole shapes in ruby using the Stark-shifting technique.

Measurements were made near the end of the pulse to avoid the small power-broadened free-induction-decay signal seen near the leading edge of the pulse. Two features to note in these results are: (i) as the intensity increases, the hole deepens and becomes increasingly power broadened, and (ii) a large decrease in the absorption coefficient is seen up to  $\sim 90 \text{ MHz}$  away from the hole.

### III. PUMP-PROBE STUDIES

#### A. Introduction

The aim of these studies was to extend the hole-burning observations to cover the entire inhomogeneous line shape. A disadvantage of the pump-probe method was that the spectral resolution was about an order of magnitude less than in the Stark studies because of the relative drifts of the two lasers. In the Stark as well as in the earlier<sup>8</sup> sideband techniques, this relative frequency drift was absent since the pump and probe beams were derived from the same source. However, since the main purpose of the experiment was to study the off-resonance saturation behavior where high resolution was not important, this deficiency was not serious.

#### B. Experimental

The pump-probe experimental setup is shown in Fig. 6. The saturating pump beam was thermally tuned and fixed near the center of the inhomogeneous line, while a counter-propagating, weak, nonsaturating probe beam was tuned to measure the inhomogeneous line shape. The probe-beam diameter was adjusted to be about three times smaller than the pump beam to minimize edge effects arising from the Gaussian beam shape and the slight misalignment between the two beams required to prevent feedback and consequent frequency instability of the lasers. Both beams were circularly polarized to observe the



#### IV. SUBSIDIARY MEASUREMENTS

For comparison of theory and experiment, knowledge of the various relaxation times and homogeneous linewidths are required. Here we present data on the spin-lattice relaxation time  $T_1$ , the magnetic field dependence of the homogeneous linewidth for the  ${}^4A_2(\pm\frac{1}{2}) \rightarrow \bar{E}(\pm\frac{1}{2})$  transition and laser-frequency-jitter measurements.

##### A. Spin-lattice time

Spin-lattice times are known to be very sensitive to the presence of impurities.<sup>14</sup> In particular  $\text{Fe}^{2+}$  and  $\text{Fe}^{3+}$  in ruby can produce orders of magnitude reduction of the  $\text{Cr}^{3+}$  relaxation time by resonant and nonresonant cross relaxation. To categorize our sample, we measured  $T_1$  by an optical technique. The two-beam method was used with the probe beam displaced  $\sim 600$  MHz from the pump beam. Pulsing the pump beam off and monitoring the recovery of the absorption coefficient by the probe yielded  $T_1$ . Over the temperature range 4.2–30 K, an inverse temperature dependence of  $T_1$  was observed as expected for a one-phonon relaxation process. The observed value of 215 msec at liquid-helium temperature is typical for a pure sample.<sup>15</sup>

##### B. Homogeneous linewidths—field dependence

Photon-echo measurements<sup>16</sup> in ruby have yielded the detailed dependence of the homogeneous linewidth as a function of  $\text{Cr}^{3+}$  concentration and magnetic field above about 500 Oe. However no accurate measurements of echo lifetimes exist for zero field. Here we present homogeneous linewidth measurements in the field range 0–200 Oe using the Stark technique for hole observation. Measurements were made at low laser power to avoid power broadening. The results are shown in Fig. 9. At zero field, the

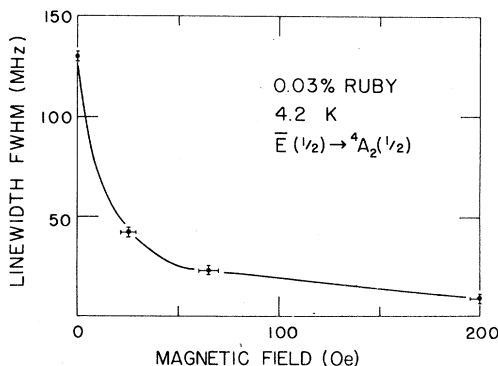


FIG. 9. Magnetic field dependence of the hole linewidth of the  ${}^4A_2(\pm\frac{1}{2}) \rightarrow \bar{E}$  transition in ruby.

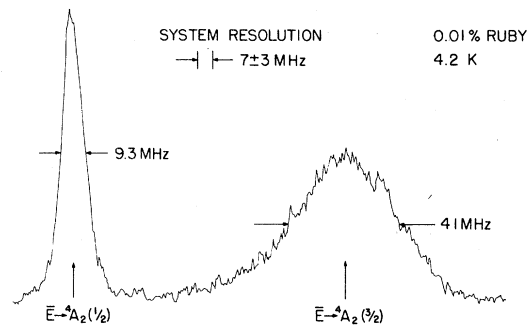


FIG. 10. Fluorescence line-narrowing spectra of 0.01% ruby in a field of 400 Oe.

FWHM homogeneous linewidth (half the observed hole width) is  $65 \pm 10$  MHz. This value agrees with FLN observations made with this sample as well as other recent Stark data.<sup>3</sup>

As an interesting aside, we see that the homogeneous linewidth of the  $\bar{E} \leftrightarrow (\pm\frac{1}{2}){}^4A_2$  and  $\bar{E} \leftrightarrow (\pm\frac{3}{2}){}^4A_2$  transitions become the same at zero field. As is well known from photon-echo studies,<sup>17</sup> when a magnetic field is applied, these transition linewidths rapidly diverge. This is also shown in the FLN results in Fig. 10 for dilute ruby in which a resolved width of  $\sim 35$  MHz is observed for the  $\bar{E} \leftrightarrow (\pm\frac{3}{2}){}^4A_2$  transition and an unresolved width  $< 5$  MHz is observed for  $\bar{E} \leftrightarrow (\pm\frac{1}{2}){}^4A_2$ . For an applied field of  $\sim 1$  kOe, recent photon-echo studies<sup>2</sup> of the present sample indicate a homogeneous linewidth of 160 kHz for  $\bar{E} \leftrightarrow (\pm\frac{1}{2}){}^4A_2$ .

##### C. Laser jitter

An important experimental parameter which arises in the comparison of theory and experiment is the laser frequency jitter; both its magnitude and the rate at which it occurs. In the present experiments, low jitter was achieved by using a new laser configuration which virtually eliminates frequency jitter arising from pump-power fluctuations.<sup>18</sup> This configuration used a very low concentration ruby (0.003%) as an oscillator to suppress pump-heating effects and a more concentrated crystal (0.05%) as an amplifier. The two systems were operated in series with the argon-ion pump-laser beam transmitted through the oscillator used to pump the amplifier.

Measurements were made with a 150-MHz free-spectral-range confocal Fabry-Perot with a 1 MHz linewidth (Burleigh model CF-500P). The peak-to-peak jitter was 1.5–2 MHz giving an rms width of  $\sim 0.7$  MHz— a value similar to that found in an earlier<sup>18</sup> study using heterodyne methods. The jitter frequency rate was in a range up to  $\sim 1$  kHz caused pri-

marily by cryostat mechanical vibrations and pointing fluctuations of the pump argon-ion laser. Unlike jet-stream dye lasers, which exhibit frequency fluctuation rates up to  $\sim 1$  MHz, such high rates were totally absent in our system since a solid block of ruby constitutes the laser cavity.

## V. THEORY

### A. Zero laser-frequency jitter

We have previously<sup>8</sup> described how cross relaxation in the ground-state levels of ruby can produce an off-resonance decrease in optical-absorption coefficient when a hole is produced in the  $R_1$  line by a monochromatic laser beam. Also, in FLN experiments in 0.03% ruby, the fluorescence inhomogeneous background was measured to be less than 1% of the line-narrowed peak. Therefore we concluded that there is no optical spectral diffusion. This conclusion on the lack of optical energy transfer between resonant and nonresonant ions is further supported by recent<sup>19,20</sup> grating experiments in ruby which show no spatial transfer beyond 30–50 nm from optically excited ions. We contend that the spatial energy transfer, which must exist to account for our results, occurs in the ground-state levels.

Our earlier<sup>8</sup> three-level model is extended here to the more realistic six-level system shown in Fig. 11. The six-level model is appropriate for  $\bar{E} \rightarrow {}^4A_2$  transi-

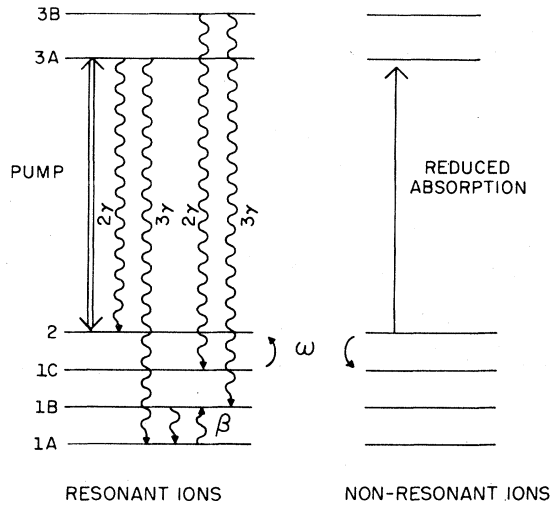


FIG. 11. Six-level model used for ruby in a magnetic field. The  $2 \rightarrow 3A$  transition is optically pumped, and coupling between the resonant and nonresonant ions occurs via cross relaxation in the four ground-state levels.  $\beta$  is the spin-lattice rate assumed equal between all levels (only two levels are shown coupled for simplicity),  $\omega$  is the cross-relaxation rate, and  $(5\gamma)^{-1}$  is the fluorescence lifetime.

tions in an applied magnetic field. In order to establish some basic rate-equation approximations, we assume initially that the ions may be divided into two groups, those resonant with the laser and those non-resonant. Using these model equations, we then formulate a theory in which a continuous frequency distribution is treated.

In Fig. 11, level 2 is the  ${}^4A_2(-\frac{1}{2})$  level which is pumped to level  $3A[\bar{E}(-\frac{1}{2})]$ . The usual ratio of  $\sigma$  spontaneous rates from the  $\bar{E}$  levels is taken, and the much slower  $\pi$  spontaneous rates are neglected. The populations of the resonant ions will be denoted by  $n_i'$ , and the nonresonant ones by  $N_i'$ . For level  $1A$  of the resonant ions we have

$$\begin{aligned} \frac{dn_{1A}'}{dt} = & -3\beta n_{1A}' + 3\gamma n_{3A}' + \beta(n_2' + n_{1C}' + n_{1B}') \\ & - \frac{\omega}{N'} [n_{1A}'(N_2' + N_{1B}' + N_{1C}') \\ & - N_{1A}'(n_2' + n_{1B}' + n_{1C}')] \end{aligned} \quad (2)$$

$\beta$  is a ground-state spin-lattice relaxation rate which is assumed to be the same between all levels so that the spin-lattice time  $T_1 = (4\beta)^{-1}$ . Actually, according to relaxation theories for ruby in which a quadratic spin-phonon Hamiltonian of the form<sup>21</sup>  $H_{SP} = \vec{S} \cdot \vec{D} \cdot \vec{S}$  produces relaxation, the latter assumption is not justified. For example, direct relaxation between the  $\pm \frac{1}{2}$  levels is forbidden as in fact has recently<sup>22</sup> been verified at very high magnetic fields (50–130 kOe). However, sizeable deviations from the theory have been seen<sup>23</sup> at lower fields such as used here. Lacking further information, we have assumed for simplicity equal spin-lattice rates between all levels. In Eq. (2),  $\omega$  is a resonant cross-relaxation rate which for 0.03% ruby is<sup>24,25</sup>  $\sim 10^6 \text{ sec}^{-1} \gg \beta \sim 1 \text{ sec}^{-1}$  (at 4.2 K) and also  $\gg \gamma = (5\tau)^{-1}$  where  $\tau$  is the  $\bar{E}$  fluorescence lifetime of  $4 \times 10^{-3}$  sec. Writing similar equations for  $n_{1B}'$  and  $n_{1C}'$ , we obtain for  $n_1' \equiv n_{1A}' + n_{1B}' + n_{1C}'$

$$\frac{dn_1'}{dt} = -\beta n_1' + 3\beta n_2' + 4\gamma n_3' - \frac{\omega}{N'}(n_1'N_2' - n_2'N_1') \quad (3)$$

where  $N'$  is the total population of off-resonance ions,  $N_1' = N_{1A}' + N_{1B}' + N_{1C}'$ , and  $n_3' = n_{3A}' + n_{3B}'$ . Because of the fast Orbach relaxation in the  ${}^2E$  levels at the temperatures in our experiments,<sup>26</sup> we take  $n_{3A}' = n_{3B}'$ . For  $N_2'$  we have

$$\frac{dN_2'}{dt} = \beta N_1' - 3\beta N_2' - \frac{\omega}{N'}(n_1'N_2' - n_2'N_1') \quad (4)$$

In equilibrium  $\dot{n}_1' = \dot{N}_2' = 0$  and from Eq. (3)

$$4\gamma n_3' \approx \frac{\omega}{N'}(n_1'N_2' - n_2'N_1') \quad (5)$$

We can neglect terms involving  $\beta$  in Eq. (3) because the spin-lattice relaxation in the ground state of the resonant  $\text{Cr}^{3+}$  ions is very much slower than the cross relaxation to the nonresonant ions. Combining Eqs. (4) and (5) gives

$$4\gamma n_3' = \beta N_1' - 3\beta N_2' \quad (6)$$

We might remark that the results obtained by using the above approximation along with the spin-temperature approximation [Eq. (14)] are identical to those obtained when the rate equations<sup>8</sup> are exactly solved for a three-level system and due approximations made because  $\omega \gg \gamma, \beta$ .

We now consider a continuous frequency dependence for the populations. Define the total population in level  $i$  by

$$n_i \equiv \int_0^\infty n_i(\nu') d\nu' \quad (7)$$

where  $\nu'$  is the optical frequency of the ion for the transition from level 2 to 3A. The absorption coefficient for this transition is

$$\alpha(\nu) = \int_0^\infty [n_2(\nu') - n_{3A}(\nu')] \sigma(\nu - \nu') d\nu' \quad (8)$$

where

$$\sigma(\nu - \nu') = \sigma_0 g_h(\nu - \nu') \quad (9)$$

and  $g_h$  is a normalized Lorentzian homogeneous-line-shape function. Rate equations for population packets at  $\nu'$  may be written

$$\begin{aligned} \frac{dn_{3A}(\nu')}{dt} = & \sigma(\nu' - \nu_L) P [n_2(\nu') - n_{3A}(\nu')] \\ & - 5\gamma n_{3A}(\nu') + R [n_{3B}(\nu') - n_{3A}(\nu')] \end{aligned} \quad (10)$$

and

$$\frac{dn_{3B}(\nu')}{dt} = R [n_{3A}(\nu') - n_{3B}(\nu')] - 5\gamma n_{3B}(\nu') \quad (11)$$

where  $R$  is the Orbach relaxation rate,  $P$  is the photon flux in photons/cm<sup>2</sup> sec, and  $\nu_L$  is the laser frequency. Adding Eqs. (10) and (11) and setting  $\dot{n}_i = 0$  gives

$$\sigma(\nu' - \nu_L) P n_2(\nu') = [10\gamma + \sigma(\nu' - \nu_L) P] n_{3A}(\nu') \quad (12)$$

Population conservation requires

$$n_1(\nu') + n_2(\nu') + n_3(\nu') = N_0 g_i(\nu' - \nu_0) \quad (13)$$

where  $N_0$  is the total population,  $g_i$  is a normalized Gaussian inhomogeneous-line-shape function, and  $\nu_0$  is the center frequency of the inhomogeneous line. Because of fast cross relaxation, we assume that all spins within the optically pumped volume come to

the same spin temperature, i.e.,

$$n_1(\nu') = f n_2(\nu') \quad (14)$$

for all  $\nu'$ , and  $f$  is a constant to be evaluated. The thermal-equilibrium value of  $f$  is  $f = 3$  in the high-temperature approximation used throughout. Equation (14) assumes a limiting size for macroscopic regions in which ions have a constant optical frequency, as will be discussed further in Sec. VII. Combining Eqs. (12)–(14) gives

$$n_{3A}(\nu') = \frac{N_0 g_i(\nu' - \nu_0)}{2 + (f + 1)[1 + 10\gamma/\sigma(\nu' - \nu_L)P]} \quad (15)$$

We write

$$n_{3A}(\nu') \equiv \frac{\epsilon N_0 g_i(\nu' - \nu_0)}{1 + 4[(\nu' - \nu_L)/\delta]^2} \quad (16)$$

where

$$\epsilon = [(1 + f)/S + (3 + f)]^{-1} \quad (17)$$

and

$$\delta = w_h \left[ S \frac{(3 + f)}{(1 + f)} + 1 \right]^{1/2} \quad (18)$$

Here  $S = \sigma_0 P / 5\gamma\pi w_h$  and  $w_h$  equals the homogeneous linewidth (FWHM).  $\delta$  is seen to be the power-broadened linewidth of the population in 3A. From these sets of equations, the frequency-dependent absorption, Eq. (8), may be evaluated

$$\alpha(\nu) = \frac{4\alpha_\mu(\nu)}{1 + f} \left[ 1 - \frac{\epsilon(3 + f)\delta(w_h + \delta)}{(w_h + \delta)^2 + 4(\nu - \nu_L)^2} \right] \quad (19)$$

where in the integration, we assume  $w_i$  [the inhomogeneous linewidth (FWHM)]  $\gg w_h$  so that  $g_i(\nu' - \nu_0)$  may be taken outside the integral.  $\alpha_\mu(\nu)$  is the unsaturated absorption coefficient.

$$\alpha_\mu(\nu) = \frac{1}{4} (\sigma_0 N_0) g_i(\nu - \nu_0) \quad (20)$$

Equation (19) describes the shape of the power-broadened hole (width =  $w_h + \delta$ ) as well as the off-resonance change in  $\alpha(\nu)$  due to cross relaxation. Our remaining task is to calculate the spin-temperature factor  $f$ . We now assume that Eq. (6) derived for a square line shape also applies for a Lorentzian line shape so that

$$4\gamma n_3 = 8\gamma n_{3A} = \beta(n_1 - 3n_2) \quad (21)$$

remembering now that  $n_i$ 's are total populations. In writing Eq. (21), we assume that the hole width is much smaller than the inhomogeneous width. Therefore we have

$$n_1 + n_2 \sim N_0 \quad (22)$$

Combining Eqs. (22) and (14) with Eq. (21) gives

$$8\gamma n_{3A} = \beta N_0 \frac{(f-3)}{(f+1)} \quad (23)$$

Integration of Eq. (16) over  $\nu'$  gives

$$n_{3A} = \frac{1}{2} \pi \epsilon \delta N_0 g_i (\nu_L - \nu_0) \quad (24)$$

Equations (17), (18), (23), and (24) may be combined to give an expression from which  $f$  may be obtained in terms of known parameters. We take the laser frequency  $\nu_L = \nu_0$ . We have

$$\frac{(f-3)^2}{(f+1)} [S(3+f) + (1+f)] = (KS)^2 \quad (25)$$

where

$$K = 8(\pi \ln 2)^{1/2} \left( \frac{\gamma}{\beta} \right) \frac{w_h}{w_i} \quad (26)$$

An experimental parameter, in which we have been particularly interested (see Fig. 7) is the fractional change in off-resonance absorption defined by

$$F \equiv \frac{\alpha_\mu(\nu) - \alpha(\nu)}{\alpha_\mu(\nu)} \quad (27)$$

where the observation frequency  $\nu$  is sufficiently far from  $\nu_L$  to be outside the hole. From Eq. (19)

$$F = \frac{f-3}{f+1} \quad (28)$$

Thus, once  $f$  is numerically evaluated from Eq. (25), experimental quantities such as  $F$  and the observed hole width  $W_h = w_h + \delta$  may be calculated.

### B. Effect of laser-frequency jitter

We calculate the effects of laser jitter in the limit of two extremes, (i) the jitter rate is much faster than the system time constants which determine the time development of the hole, and (ii) the jitter rate is much slower than these time constants. For simplicity, a time-averaged Lorentzian shape for the jitter-broadened laser line shape is assumed.

Consider first fast jitter. In this model we write for the spectral distribution of  $P$  in Eqs. (10) and (11)

$$P(\nu'') = P_0 g_J(\nu'' - \nu_L) \quad (29)$$

where

$$g_J(\nu'' - \nu_L) = \frac{2J}{\pi [J^2 + 4(\nu'' - \nu_L)^2]} \quad (30)$$

Here  $J$  is the laser-jitter linewidth (FWHM). On integration over  $\nu''$  in Eqs. (10) and (11), this simply results in a convolution of  $J$  with  $w_h$  so that all the earlier analysis may include jitter by replacing

$w_h \rightarrow w_h + J$ . The hole width  $W_h$  in Eq. (19) becomes

$$W_h = (w_h + J) \left[ 1 + \left( \frac{S(3+f)}{(1+f)} + 1 \right)^{1/2} \right] \quad (31)$$

which in the limit of low power ( $S \rightarrow 0$ ) becomes  $W_h = 2(w_h + J)$  as might be physically expected.

The case of slow jitter is more difficult to treat and we proceed intuitively. Looking at the line shape for the  $n_{3A}$  population in Eq. (16), we replace

$$\delta \rightarrow \delta + J \quad (32)$$

i.e., the Lorentzian jitter width simply adds to the power broadened width  $\delta$ . The next question is, how is  $\epsilon$  modified by the jitter? To first order, we expect  $\epsilon$  to be independent of jitter. In other words as the laser frequency moves about, the peak of the  $n_{3A}$  population remains at the no-jitter value. This is what we mean by "slow" jitter. These considerations change Eq. (25) for  $f$  to the equation

$$\begin{aligned} \frac{(f-3)^2}{(f+1)} [S(3+f) + (1+f)] \\ = (KS)^2 \left[ 1 + \frac{J}{w_h} \left( \frac{(1+f)}{S(3+f) + (1+f)} \right)^{1/2} \right]^2 \end{aligned} \quad (33)$$

Since the probe laser also exhibits a jitter  $J$ , the width of the observed hole from Eq. (19) becomes

$$W_h = 2J + w_h \left[ 1 + \left( \frac{S(3+f)}{(1+f)} + 1 \right)^{1/2} \right] \quad (34)$$

which again approaches the proper limit  $2(w_h + J)$  in the limit of low power.

## VI. COMPARISON OF THEORY AND EXPERIMENT AND DISCUSSION

Comparison of theory with experiment for the off-resonance fractional change in absorption  $F$ , the hole

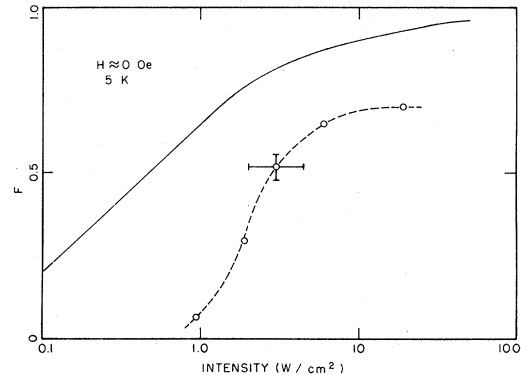


FIG. 12. Comparison of theory (—) and experiment (-o-) for the fractional change  $F$  in off-resonance absorption coefficient for zero field.

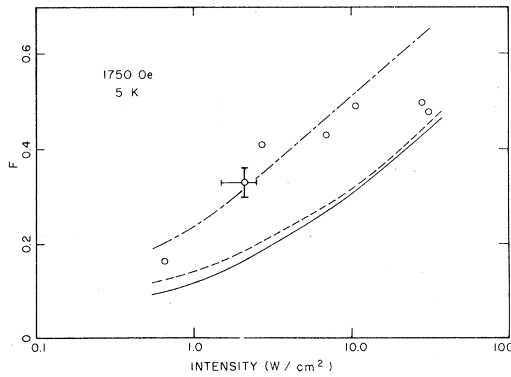


FIG. 13. Comparison of theory and experiment (O) for the fractional change  $F$  in off-resonance absorption coefficient vs pump intensity for an applied magnetic field along the  $c$  axis. Theoretical curves (1) no laser jitter —, (2) slow laser jitter of width 0.7 MHz FWHM ---, (3) fast laser jitter of width 0.7 MHz FWHM -·-·.

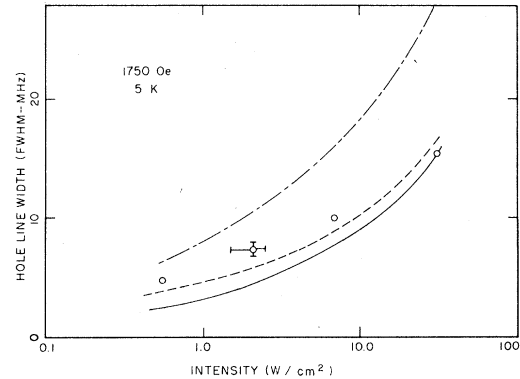


FIG. 14. Comparison of theory and experiment (O) for the holewidth (FWHM) vs pump intensity for an applied magnetic field along the  $c$  axis. Theoretical curves (1) no laser jitter —, (2) slow laser jitter of width 0.7 MHz FWHM ---, (3) fast laser jitter of width 0.7 MHz FWHM -·-·.

width, and the temperature dependence of  $F$  is given in Figs. 12–14 and in Fig. 8. These are discussed in the following paragraphs.

#### A. Zero-field studies— temperature dependence

The two parameters in the theory which are temperature dependent are  $T_1$  and the homogeneous linewidth. The direct process and Raman-induced phonon linewidths were calculated from the theory of McCumber and Sturge<sup>27</sup> using the photon-echo-derived<sup>28</sup> direct process coefficient  $\beta' = 8.1 \text{ cm}^{-1}$  and the Raman coefficient  $\alpha' = 544 \text{ cm}^{-1}$ . The phonon-induced linewidth was then added to the homogeneous linewidth of 65 MHz measured at 5 K. The calculated variation of  $F$  with temperature is shown in Fig. 8 along with experimental data. The observed decrease in  $F$  with increasing temperature is qualitatively predicted by the theory; however, the theoretical curve lies well above the observed points. A similar deviation is also observed in Fig. 12 where the power dependence of  $F$  is shown for zero magnetic field.

The  $F$  values in an applied field (Fig. 13) are smaller than in zero field (Fig. 12). This is qualitatively explained by the theory as arising from the larger homogeneous linewidth in zero field.

One assumption of our theory which could explain part of the discrepancy at low powers (small saturation) is simply that our sample is not optically thin. However if we assume a worst-case situation in which the smallest measured intensity is attenuated by a factor of 5 (corresponding to the unsaturated attenuation), the theoretical  $F$  value still exceeds the experimental value. Another possibility is that the six-level model is no longer appropriate at zero field.

We believe, however, that a major source of the discrepancy is related to the question of the nature of the line broadening produced by the superhyperfine interaction between the Al and Cr spins. As discussed by Grischkowsky and Hartmann,<sup>29</sup> this broadening arises from the time-dependent magnetic field at the Cr site produced by the flipping Al spins of the host lattice. This produces a modulation  $m(t)$  of the Cr energy-level separation, which has a minimum value when a magnetic field is applied along the  $c$  axis ( $\theta = 0^\circ$ ). As qualitatively confirmed in the FLN results of Fig. 12, this broadening will be larger for  ${}^4A_2(\pm \frac{3}{2}) \rightarrow \bar{E}$  transitions than for  ${}^4A_2(\pm \frac{1}{2}) \rightarrow \bar{E}$  transitions because of the different splitting rates  $\delta\nu/\delta H$ . When  $\theta \neq 0^\circ$ ,  $m(t)$  rapidly increases because the Al precession axes no longer approximately coincide with the Cr precession axes. This results in an increase of the projection of the time-dependent part of the Al spin vector on the Cr spin vector, hence increasing  $m(t)$ . This feature is responsible for the increase in linewidth at zero field. An unknown factor is the nature of the time dependence of  $m(t)$  which is determined by the complex Cr-Al-Al spin interactions. As discussed by Shelby *et al.*<sup>30</sup> for the system  $\text{Pr}^{3+}:\text{LaF}_3$ ,  $m(t)$  may exhibit a slow component, since Al spins near the Cr ions will be detuned from distant Al spins, and hence their flip-flop rate will be much slower than those of the distant spins. This idea that superhyperfine broadening has an approximately static inhomogeneous component along with a homogeneous component is supported by recent hole-burning observations<sup>5</sup> in  $\text{Pr}^{3+}:\text{LaF}_3$  which gave a frequency-domain linewidth of 200 kHz compared to the time-domain width of 20 kHz inferred from coherent transient studies.<sup>7,30</sup> It is tempting to model the 65-MHz width of ruby in zero field as arising from a smaller homogeneous width

plus an "atomic jitter" width. Unfortunately accurate echo data do not exist for ruby at zero field to test this idea. Assuming slow jitter, this kind of model could bring theory closer to the data by varying  $w_h$  and  $J$ , where  $J$  is now identified as the atomic jitter.

### B. Magnetic-field studies

Comparison of theory and experiment for the two laser-jitter models are shown in Figs. 13 and 14. Fair agreement between experiment and theory is obtained assuming that fast jitter occurs at low power levels and slow jitter applies at high power levels. This is consistent with the idea that the hole-formation time is expected to shorten with increasing power.

Regarding atomic-jitter, a similar problem exists as in Sec. VI A in that no high-resolution data exist for the width one would see in the frequency domain. The 160-kHz ( $T_2 \sim 2 \mu\text{sec}$ ) width inferred<sup>2</sup> for our ruby from echo studies is presumably produced by resonant cross relaxation<sup>31</sup> since  $T_2 \sim \omega^{-1} \sim 1 \mu\text{sec}$ . It might be mentioned that calculations<sup>1,17,32</sup> of Al superhyperfine broadening in a magnetic field predict a width of  $\sim 0.5$  MHz using an approach developed by Wenzel<sup>33</sup> for EPR broadening. However, this theory does not consider the time dependence of the Al spin flips. The width is calculated taking random static Al spin configurations around the Cr ion. Since photon-echo measurements have yielded<sup>16</sup> linewidths as narrow as 25 kHz in dilute ruby at high magnetic field, it seems clear that the linewidth calculated from the static approach is in fact inhomogeneous.

## VII. FURTHER COMMENTS AND CONCLUSIONS

Despite the lack of agreement between theory and experiment for some of our observations, we believe that cross relaxation is the major mechanism which produces the large change in off-resonance absorption coefficient. This is further supported by observation of small increases in  $F$  for magnetic field values at which the ground-state energy-level spacings are harmonically related. (See note added in proof.) As is well known from EPR studies, additional cross relaxation occurs<sup>34</sup> under such conditions.

We might emphasize that in the field of spin thermodynamics, the present studies represent a rather unique situation in which spins labeled by a particular optical frequency are initially driven by optical pumping to a temperature far different from the non-resonant spins. Our significant observation that *all* spins within the pumped volume come to the same temperature has interesting implications regarding the spatial distribution of ions having the same optical frequency or in other words on the question of ma-

croscopic versus microscopic inhomogeneous broadening in ruby. By macroscopic broadening we mean the existence of regions in which all ions have the same optical frequency as opposed to microscopic for which the frequency varies randomly from site to site. This question is of importance in recent speculations<sup>35-37</sup> of the possible occurrence of an Anderson transition in ruby. An approximate upper limit on the size of macroscopic regions may be calculated. The number of Cr spin flip flops which occur before thermalization occurs by a phonon interaction is  $\omega T_1 \approx 2 \times 10^5$ . Assuming a random-walk model and a step distance  $l \sim 2.6 \times 10^{-7}$  cm for 0.03% ruby calculated from Lyo's<sup>35</sup> formula  $l^3 = 0.17/N_0$ , we obtain a diffusion distance of

$$(2.6 \times 10^{-7})(2 \times 10^5)^{1/2} = 1200 \text{ nm} ,$$

which represents the maximum size of macroscopic regions. Also, since this distance is much less than the diameter of the pumped filament ( $\sim 3 \times 10^{-3}$  cm), significant thermalization of the pumped spins by the unpumped spins outside the filament is not expected. As the sample temperature increases, the diffusion distance decreases because of the decrease in  $T_1$ . It is possible that the anomalously low  $F$  values observed at higher temperature may arise because the diffusion distance becomes less than the macroscopic region dimension. However, the generally low  $F$  values seen at zero field do not permit a firm conclusion.

In summary, an earlier<sup>8</sup> hypothesis that ground-state cross relaxation occurs over only part of the  $R_1$  inhomogeneously broadened line in ruby is incorrect. Using a simple three-level model and a square hole shape, this earlier hypothesis seemed to be necessary to correlate theory with the large observed decrease in absorption coefficient outside the hole. However, the present studies show that reasonable agreement between a more sophisticated theory and experiment is obtained for cross relaxation over the *entire* inhomogeneous line. The latter observation places an upper limit of 1200 nm on the size of macroscopically broadened regions in ruby. Further studies are needed to elucidate the nature of the  $R_1$  line broadening mechanisms in ruby due to Al superhyperfine interactions to explain some aspects of the observed optical saturation behavior.

*Note added in proof.* A similar observation using a different technique has also been reported by A. C. Boccara; Colloq. Int. CNRS 255, 299 (1977).

## ACKNOWLEDGMENTS

We thank L. E. Erickson for commenting on the manuscript and M. Kroll and E. L. Dimock for technical assistance in the experiments.

- \*On leave from Faculty of Education, Shiga University, Otsu, Japan 520.
- <sup>1</sup>A. Szabo, Phys. Rev. Lett. 25, 924 (1970); 27, 323 (1971).
  - <sup>2</sup>A. Szabo and M. Kroll, Opt. Commun. 18, 224 (1976); A. Szabo and M. Kroll, Opt. Lett. 2, 10 (1978).
  - <sup>3</sup>T. Muramoto, S. Nakanishi, and T. Hashi, Opt. Commun. 21, 139 (1977).
  - <sup>4</sup>R. M. Shelby and R. M. Macfarlane, Opt. Commun. 27, 399 (1978).
  - <sup>5</sup>L. E. Erickson, Phys. Rev. B 16, 4731 (1977).
  - <sup>6</sup>I. D. Abella, N. A. Kurnitt, and S. R. Hartmann, Phys. Rev. 141, 391 (1966).
  - <sup>7</sup>R. G. De Voe, A. Szabo, S. C. Rand, and R. G. Brewer, Phys. Rev. Lett. 42, 1560 (1979).
  - <sup>8</sup>A. Szabo, Phys. Rev. B 11, 4512 (1975); A. Szabo, IEEE J. Quantum Electron. QE-10, 747 (1974).
  - <sup>9</sup>A. Gorokhovski, R. K. Kaarli, and L. A. Rebane, JETP Lett. 20, 216 (1974).
  - <sup>10</sup>H. de Vries and D. A. Wiersma, Phys. Rev. Lett. 36, 91 (1976).
  - <sup>11</sup>R. M. Macfarlane and R. M. Shelby, Phys. Rev. Lett. 42, 788 (1979).
  - <sup>12</sup>A. Szabo, US Patent 3,896,420, *Frequency selective optical memory*, 1975; G. Castro, D. Haarer, R. M. Macfarlane, and H. D. Trommsdorff, US Patent 4,101,976, *Frequency selective optical data storage system*, 1978. See also Laser Focus 14, 30 (1978).
  - <sup>13</sup>M. G. Cohen and N. Bloembergen, Phys. Rev. 135, A950 (1964).
  - <sup>14</sup>C. A. Bates, A. Gavaix, P. Stegges, A. Vasson, and A-M Vasson, J. Phys. C 8, 2300 (1975).
  - <sup>15</sup>K. J. Standley and R. A. Vaughan, Phys. Rev. 139, A1275 (1965).
  - <sup>16</sup>P. F. Liao and S. R. Hartmann, Opt. Commun. 8, 310 (1973).
  - <sup>17</sup>L. Q. Lambert, Phys. Rev. B 7, 1834 (1973).
  - <sup>18</sup>A. Szabo, J. Appl. Phys. 46, 802 (1975).
  - <sup>19</sup>D. S. Hamilton, D. Herman, J. Feinberg, and R. W. Hellwarth, Opt. Lett. 4, 124 (1979).
  - <sup>20</sup>P. F. Liao, L. M. Humphrey, D. M. Bloom, and S. Geschwind (unpublished).
  - <sup>21</sup>R. Orbach and H. J. Stapleton, in *Electron Paramagnetic Resonance*, edited by S. Geschwind (Plenum, New York, 1972), p. 121.
  - <sup>22</sup>A. Misu, J. Phys. Soc. Jpn. 44, 1161 (1978).
  - <sup>23</sup>R. A. Lees, W. S. Moore, and K. J. Standley, Proc. Phys. Soc. London 91, 105 (1967).
  - <sup>24</sup>R. L. Khyll and B. D. Nageswara-Rao, Phys. Rev. 158, 284 (1967).
  - <sup>25</sup>V. A. Atsarkin, Sov. Phys. Solid State 17, 1582 (1975).
  - <sup>26</sup>S. Geschwind, G. E. Devlin, R. L. Cohen, and S. R. Chinn, Phys. Rev. 137, 1087 (1967).
  - <sup>27</sup>D. E. McCumber and M. D. Sturge, J. Appl. Phys. 34, 1682 (1963).
  - <sup>28</sup>N. A. Kurnitt, I. D. Abella, and S. R. Hartmann, in *Physics of Quantum Electronics*, edited by P. L. Kelly, B. Lax, and P. E. Tannenwald (McGraw-Hill, New York, 1966), p. 267.
  - <sup>29</sup>D. Grischkowsky and S. R. Hartmann, Phys. Rev. B 2, 60 (1970).
  - <sup>30</sup>R. M. Shelby, C. S. Yannoni, and R. M. Macfarlane, Phys. Rev. Lett. 41, 1739 (1978).
  - <sup>31</sup>A. Compaan, Phys. Rev. B 5, 4450 (1972).
  - <sup>32</sup>P. F. Liao, P. Ho, R. Leigh, and S. R. Hartmann, Phys. Rev. A 9, 332 (1974).
  - <sup>33</sup>R. F. Wenzel, Phys. Rev. B 1, 3109 (1970).
  - <sup>34</sup>K. J. Standley and R. A. Vaughan, *Electron Spin Relaxation Phenomena in Solids* (Hilger, London, 1969).
  - <sup>35</sup>S. K. Lyo, Phys. Rev. B 3, 3331 (1971).
  - <sup>36</sup>J. Koo, L. R. Walker, and S. Geschwind, Phys. Rev. Lett. 35, 1669 (1975).
  - <sup>37</sup>P. M. Seltzer, D. L. Huber, B. B. Barnett, and W. M. Yen, Phys. Rev. B 17, 4979 (1978).